Manuscript Click here to view linked References

Hydrophilic Domains Compose of Interlocking Cation-π Blocks for Constructing Hard Actuator with Robustness and Rapid Humidity Responsiveness

Yicheng Li,[†ab] Mengqi Du,[†a] Li Yang,[ac] Yunjia Bao,[a] Yewei Xu,[a] Qiang Yin,[b] Yang Lan,[d] and Guanjun Chang*[ac]*

[a] State Key Laboratory of Environment-friendly Energy Materials & School of Material Science and Engineering, Southwest University of Science and Technology, Mianyang, 621010, P. R. China. E-mail: gjchang@mail.ustc.edu.cn

[b] Research Center of Laser Fusion, China Academy of Engineering Physics, Mianyang, 621900, P. R. China.

[c] Department of Chemical and Biomolecular Engineering, University of Pennsylvania, Philadelphia, Pennsylvania, 19104, USA. E-mail: yanglichem628@126.com

[d] Department of Chemical Engineering, University College London, Torrington Place, London, WC1E7JE, UK.

† Yicheng Li and Mengqi Du contributed equally to this work.

KEYWORDS: actuators, hydrophilic domains, robustness, rapid humidity responsiveness, cation-π interactions

Abstract

Biomimetic actuators have seemingly infinite potential for use in previously unexplored areas. However, large stresses and a rapid water response are difficult to realize in soft actuators, owing to which their practical applicability is currently limited. In this paper, a new method for designing and fabricating humidity-responsive sturdy hard actuator. By combining a rigid matrix and hydrophilic water domains consisting of dynamic interlocking cation-π blocks, high-performance polymer actuator was synthesized that swell rapidly in response to a water gradient in their environment, resulting in unprecedentedly large stresses. More critically, the strong interlocking cation-π blocks reform and the intermolecular distance is reduced when the water is removed, allowing the deformed actuator to revert its original shape. The proposed design principle can potentially be extended to produce different types of sturdy actuators with rapid water responsiveness.

1. Introduction

For animals, self-adaptive behaviours in response to external stimuli from exposure to humidity, light, temperature, and other natural conditions, are always essential for survival [1,2]. Most of such responsive behaviours are mainly due to nonuniform internal structures after stimulation including different density, expansion/contraction, and swelling volume. Inspired by these biological systems, a serious of soft actuators with inherent stimuli responsiveness have been developed, and are well suited for application including but not limited to sensors [3], artificial muscles [4,5], soft robots [6-8], and microfluidic switches [9,10] correspondingly. In a typical case, humidity-driven soft actuators process self-adaptive movements through different swelling/shrinkage in parallel and vertical directions [11,12]. Although humidity-driven soft actuators have made considerable progresses, their fact application still faces big challenges [13].

Commonly focus is on response bending speed, yet the key problem of humidity-driven soft actuators is the amplified combination of bend speed and stress [14-16]. However, the current development of sturdy actuators are limited to the flexible polymer [17-19]. From this point of view, when it comes to the resistance, the actuators in progress may be interrupted or terminated owing to low modulus and weak stress generation of flexible polymer chains, causing blocked process of grasping heavy objects. Among many the uncertainties in practice, an integrated performance of high modulus, robustness, and rapid humidity responsiveness actuators is required to achieve basic functions (bending, rotation, and twist). It is known that the incorporation of a stiff polymer frame can improve the stress generation capability and modulus [20-22]. There is another issue arose that water molecules is difficult to enter the interior from the surface owing to its dense stiff polymer and weak segment mobility, which cause greatly reduce the humidity sensitivity. Accordingly, the construction of a new generation of high-performance rigid polymer actuators assembled with robustness and rapid humidity responsiveness, would be a promising and attractive challenge.

In this work, we describe a new concept for designing sturdy, fast-swelling hard actuators based on the construction of a series of hydrophilic water domains (Fig. 1A), through which water molecules can enter the actuator quickly (Fig. 1B). These hydrophilic water domains consist of a large number of tryptophan salts in the form of interlocking cation-π blocks, which are hydrated readily [23-29]. When water molecules enter these domains, the interlocking cation-π blocks are destroyed. Further, with an increase in the number of water molecules within the domains, the tryptophan segments in the stiff polymer frame start facing away from each other, resulting in a high degree of swelling of the frame (Fig. 1C) [30-32]. Thus, water-gradient-based swelling is achieved during the transfer of the water molecules from one side of the hard actuator to the other,

resulting in the generation of a large stress in the direction of water transportation. This stress is essential for the bending of the actuator. While the recovery of stiff polymeric actuator is an essential characteristic, it is actually difficult to realize this characteristic in such polymer owing to its poor segment mobility. As the water molecules continually migrate from the inside of the actuator to its surface and evaporate at the surface, the tryptophan segments gradually approach each other again, driven by the reformation of the strong interlocking cation-π blocks. This causes the actuator to revert to its original shape (Fig. 1B). Thus, this approach based on hydrophilic interlocking cation-π blocks can help overcome the limitations related to the trade-off between generating large stresses and exhibiting high water sensitivity that are encountered in the case of stiff polymer. We believe that this method will be suitable for designing and fabricating advanced actuators combining high modulus, robustness, and rapid humidity responsiveness.

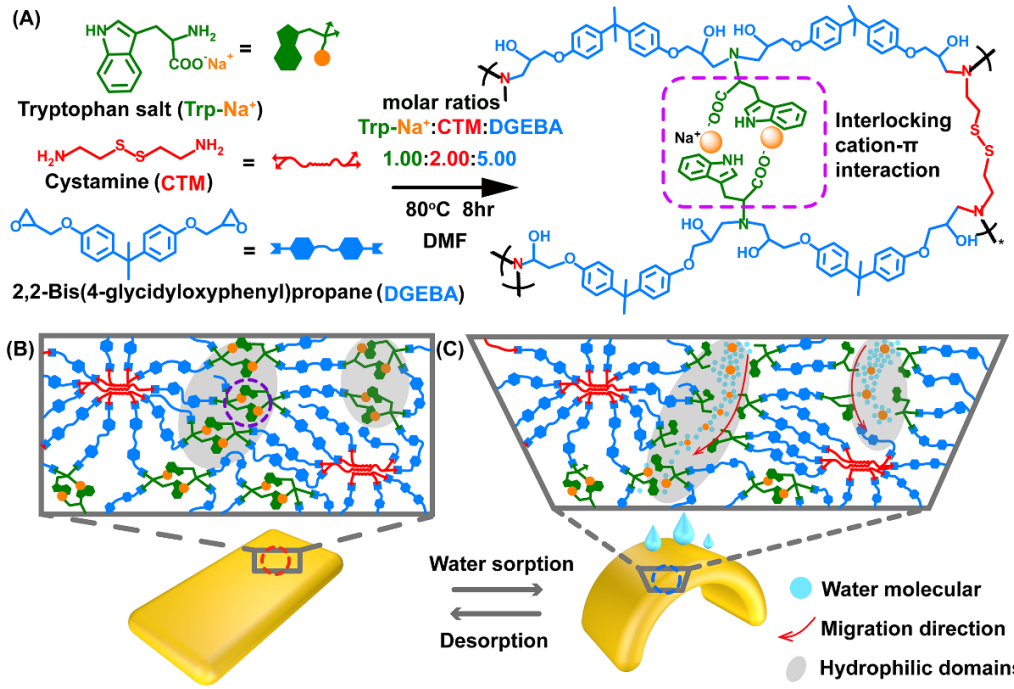

Fig. 1 Scheme and synthesis of hard actuator that exhibit water-gradient-based swelling. (A) Synthesis of stiff epoxy polymer ($PIN^{(1/2)}$) with interlocking cation-π blocks by solution casting and heat curing of Trp-Na^+, CTM, and DGEBA in DMF for use in fabrication of hard actuator; (B) and (C) in $PIN^{(1/2)}$ actuator, aggregated S-S bonds of CTM act as dynamic crosslinkers driven by hydrophobic interactions and improve static structural support. Interlocking cation-π domains consisting of interlocking cation-π blocks quickly adsorb and transport water molecules from side in contact with water. With water desorption, strong interlocking cation-π blocks reform and intermolecular distance is reduced, causing actuator to revert to original shape.

2. Results and discussion

2.1 Synthesis and characterization of stiff polymer films ($PIN^{(x)}$)

To demonstrate the proposed concept, we fabricated free-standing actuator of an epoxy polymer by the solution casting of cystamine (CTM), a tryptophan salt (Trp-Na^+), and 2,2-bis(4-glycidyloxyphenyl) propane (DGEBA) in N,N-dimethylformamide (DMF), which were then used to construct hard actuator (Fig. 1A and Table S1). It was confirmed that the carboxyl group of tryptophan was deprotonated by ^{1}H NMR (Fig. S2). The copolymers are denoted as $PIN^{(x)}$, where x is the molar ratio of Trp-Na^+ to CTM in the feed. The methods used for characterizing these polymers are described in Supporting Information. That the rate of epoxy conversion was high was confirmed through Fourier transform infrared spectroscopy (Fig. S3). With an increase in the Trp-Na^+-to-CTM molar ratio in the feed, the sample exhibited changes in their macroscopic properties (Fig. S4–S7). The structural information of the prepared $PIN^{(1/2)}$ was also obtained by ^{13}C CP/MAS NMR (Fig. S5). There are three broad signals at 105-120 ppm ascribed to the indole and benzene group carbons. The signal at about 58 ppm corresponds to carbons on aliphatic chain. In addition, the mechanical behaviors of the sample also varied with the Trp-Na^+-to-CTM ratio. As can be seen from Fig. S8, the $PIN^{(1/2)}$ sample showed the highest tensile strength and toughness and was thus the most suitable for fabricating hard actuator. Thus, we used the $PIN^{(1/2)}$ sample for the rest of the study. In this work, the different functional groups present in the $PIN^{(1/2)}$ actuator endowed the fabricated hard actuator with different functionalities. On the one hand, the aggregation of the disulfide bonds (S-S bonds) of CTM owing to hydrophobic interactions allowed for becoming crosslink points to fix the shape of hard actuator and the configuration of the two-dimensional (2D) actuator into different 3D shapes through a thermoreversible bond exchange [33–36]. On the other hand, the reversible interlocking cation-π blocks allowed the mechanical behavior of the stiff

PIN$^{(1/2)}$ polymer actuator to change with the sorption and desorption of water (Fig. 1B and 1C). Given these functionalities of the PIN$^{(1/2)}$ actuator, we investigated its mechanical behavior in detail by varying its local water environment and analyzing the effect on its dependent properties, including its hygroscopicity and the magnitude of the contractile force and stress generated.

2.2 Confirmation of presence of reversible interlocking cation-π blocks

We performed simulations and experiments to study the effects of the presence of external water on the formation of interlocking cation-π blocks between the indole-based units. Specifically, we performed a series of quantum dynamics (QD) and all-atoms molecular dynamics (MD) simulations to study the equilibrium conformation of PIN$^{(1/2)}$ in the presence and absence of water molecules [37-41]. The radial distribution function as calculated through the MD simulations indicated a strong correlation between the indole units and Na^+ ions at a distance of 3.67 Å, resulting in the formation of an interlocking cation-π structure consisting of two Try-Na^+ segments (Fig. 2A). After the water treatment, the Na^+ ions were surrounded by water molecules, resulting in a significant increase in the distance between the Na^+ ions and the indole units. This was because the hydration energy of Na^+ ions (-24.73 kcal mol^{-1}) is significantly higher than the energy of the bonds between the Na^+ ions and the indole units (-20.45 kcal mol^{-1}) (Fig. 2BE) [30]. To verify the reversibility of the interlocking cation-π structure, the equilibrium conformation of the PIN$^{(1/2)}$ polymer was studied after the removal of the water molecules. The results showed that the distance between the Na^+ ions and the indole units decreased to 3.79 Å (Fig. 2C) within the cation-π distance around 3.5−4.5 Å (Fig. 2D) according to cation-aromatic database (CAD), resulting in the reformation of the interlocking cation-π structure. Therefore, we were able to theoretically demonstrate the controllability of the interlocking cation-π blocks using an external water treatment. Ultraviolet-visible (UV-vis) absorption spectroscopy is a useful method for structural

investigations of both solid and liquid packing and was used to elucidate the cation-π interactions [41,42]. Fig. 2F shows the absorption spectra of the $PIN^{(1/2)}$ and $PIN^{(1/2)}$+H_2O samples, along with their difference spectrum. The UV difference spectrum exhibits a distinct negative/positive band pair at approximately 231/244 nm, thus confirming the formation of interlocking cation-π blocks between the Na^+ ions and the indole rings. After the removal of the water molecules from the $PIN^{(1/2)}$ samples, the interlocking cation-π blocks reformed within the polymer network. This was further confirmed by the difference spectrum of the $PIN^{(1/2)}$+H_2O and dried $PIN^{(1/2)*}$ samples (Fig. 2G). Thus, the changes in the macroscopic properties of the $PIN^{(1/2)}$ actuators can be ascribed to the presence of the reversible interlocking cation-π blocks (Fig. 2H).

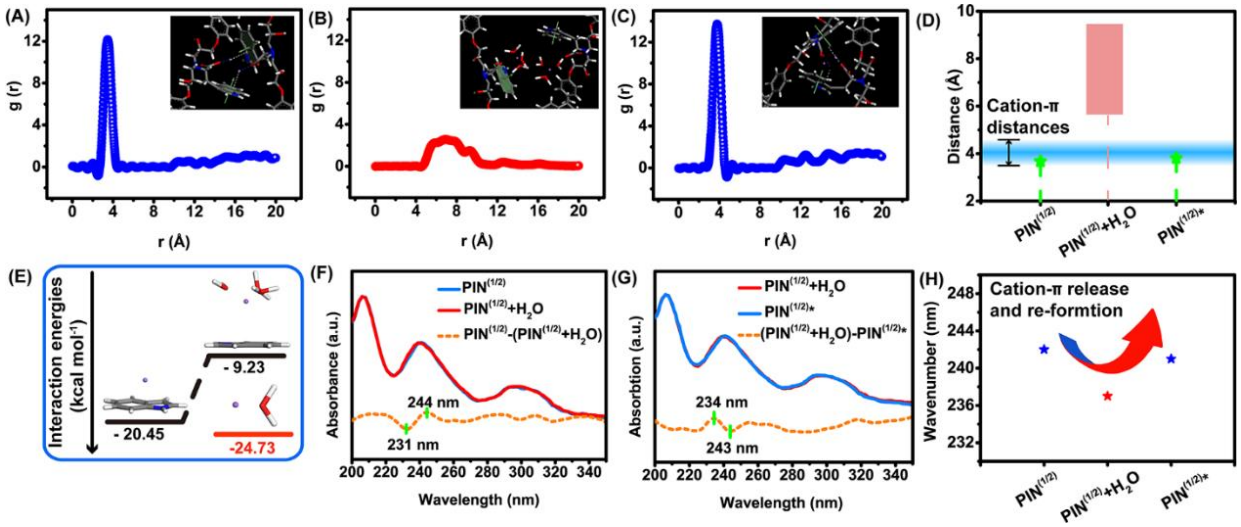

Fig. 2 Radial distribution of Na^+ ions as function of distance from indole groups in (A) $PIN^{(1/2)}$, (B) $PIN^{(1/2)}$ after water uptake ($PIN^{(1/2)}$+H_2O), and (C) $PIN^{(1/2)}$ after desorption of water ($PIN^{(1/2)*}$); insets show snapshots of two highlighted adjacent polymer chains in MD simulation box in equilibrium state; (D) summary of the distance of Na^+ and indole unite and the distance range of cation-π interactions; (E) interaction energies of indole units and cations under hydration and without it (black line); interaction energy of water molecule with Na^+ ion (red line); (F) and (G) UV-vis absorption spectra of $PIN^{(1/2)}$, $PIN^{(1/2)}$+H_2O, and $PIN^{(1/2)*}$ actuator, difference spectra of (F) $PIN^{(1/2)}$ and $PIN^{(1/2)}$+H_2O actuator and (G) $PIN^{(1/2)}$+H_2O and $PIN^{(1/2)*}$ actuators; (H) summary of fluctuations of UV-vis absorption peak shift related to cation-π interaction from Fig. 2F and G.

2.3 Hydrophilic domains for adsorption of water molecules

We assumed that it would be possible to form hydrophilic domains for the adsorption of water molecules by the nanophase separation of the hydrophilic Try-Na^+ segments and the hydrophobic

blocks and that these domains would allow for the rapid absorption of water molecules within the stiff polymer frame. The morphology of the PIN$^{(1/2)}$ sample by spin coating (Fig. 3C) was investigated using transmission electron microscope (TEM). Fig. 3A shows that the phase separation of the hydrophilic (dark regions) and hydrophobic (brighter regions) domains did occur during pellicle formation, owing to the repulsion between the hydrophobic blocks and the hydrophilic Try-Na$^+$ segments [24-29]. Circular ionic domains with an approximate size of 30–50 nm were uniformly distributed within the PIN$^{(1/2)}$; these played an important role in the absorption of water molecules. For comparison, the morphology of a PIN$^{(0)}$ without the hydrophilic Try-Na$^+$ segments in its polymer chains was also studied using TEM (Fig. S9B). We found that the PIN$^{(0)}$ exhibited a homogeneous morphology. In other words, no water hydrophilic domains were present in the PIN$^{(0)}$. The bent PIN$^{(1/2)}$ actuator was rapidly immersed in liquid nitrogen to limit the changes in the conformation of its polymer chains. After the actuator had been freeze-dried, it was subjected to TEM imaging again. It was found that the hydrophilic domains were "elongated" (Fig. 3B). Molecular dynamics simulations were performed in Materials Studio 2019 for morphology analysis of PIN$^{(1/2)}$ [43]. The affinity between tryptophan, water and Na$^+$ leaves exposed the functional groups to the hydrophilic domains, while hiding the hydrophobic regions of the polymer, leading to the formation of hydrophilic domains (Fig. 3D). Aggregation of Na$^+$ mapping was shown in Fig. 3E, which is main components of hydrophilic domains.

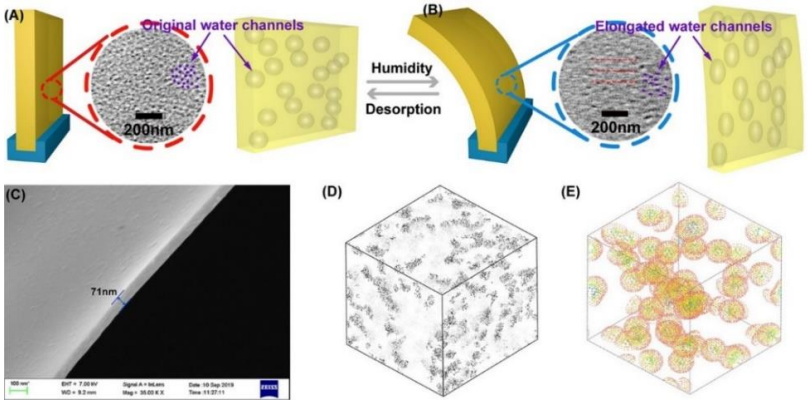

Fig. 3 (A) and (B) TEM images showing phase separation of PIN$^{(1/2)}$ hard actuator and its morphology before and after water treatment; (C) the thickness of PIN$^{(1/2)}$ hard actuator by spin coating used to TEM characteration; Equilibrated boxs of (D) PIN$^{(1/2)}$ and (E) aggregation of Na^+ mapping. The polymer chain is hiding, and hydrophilic domains are shown in dark color.

2.4 Robustness and rapid actuation of polymer actuators

To investigate the hygroscopicity of the PIN$^{(1/2)}$ actuators, we prepared rectangle PIN$^{(1/2)}$ strips (25 mm × 5 mm × 0.5 mm) and analyzed their humidity sorption ratios, bending kinetics, and reversibility characteristics (see Materials and methods). When the PIN$^{(1/2)}$ strip reached the point of saturation, which occurred within 65 s at an external relative humidity (RH) of 99%, the maximum humidity sorption ratio reached 13.7±0.6 wt% (Fig. 4A). For comparison, the humidity sorption ratios of PIN$^{(0)}$ strips that did not contain the hydrophilic tryptophan segments within the polymer network were also measured; these were very low at 1±0.2 wt%. Thus, it can be concluded that the hydrophilic domains consisting of interlocking cation-π blocks played an important role in the absorption of water molecules.

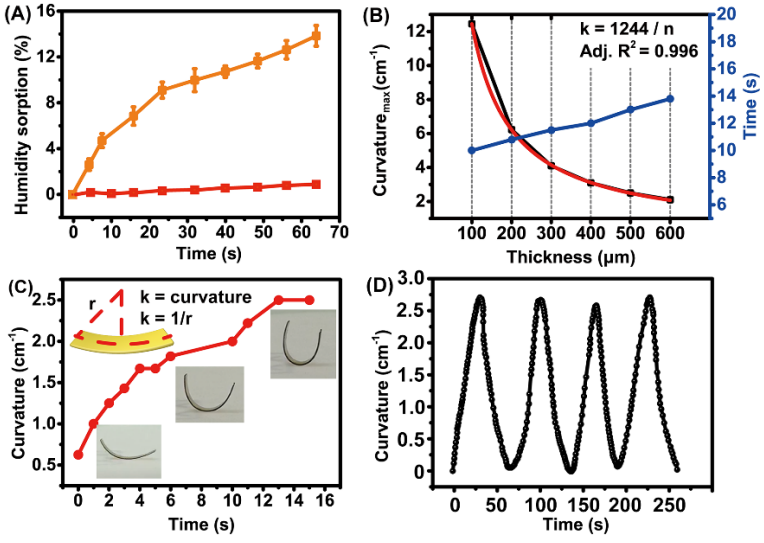

Fig. 4 (A) Humidity sorption ratio of completely dry PIN$^{(0)}$ actuator (red line) and PIN$^{(1/2)}$ actuator (orange line) placed in humid environment (RH = 99%); (B) maximum curvatures of PIN$^{(1/2)}$ actuators with different thicknesses and times required to reach them as determined using method shown in Fig. 4C; (C) quantitative analysis of hygroscopicity; (D) quantitative analysis of controllable and reversible deformation of PIN$^{(1/2)}$ actuators.

Increasing the thickness significantly increased the amount of elastic potential energy generated during swelling (see Materials and methods). However, it also reduced the water responsiveness [45]. We performed a series of bending tests on $PIN^{(1/2)}$ actuator of different thicknesses (100–600 μm) using the method shown in Fig. 4B and measured their maximum curvature and the corresponding time. The results showed that the maximum curvature, k, is proportional to $1/n$ (where n is the thickness) (Fig. 4B). This proportionality relationship indicated that neither the formation of the water gradient within the $PIN^{(1/2)}$ actuator when bent to their maximum curvature (Equation 1 in Materials and methods) nor the time required for bending (10–14 s) was affected by the thickness (Fig. 4B). Further, as expected, owing to the presence of the highly sensitive hydrophilic domains, the $PIN^{(1/2)}$ actuator with the different thicknesses all exhibited fast bending, with the bending speed being comparable to those of other similar thin, soft actuator (<50 μm) [44-49]. However, for the same humidity level, increasing the thickness decreased the maximum bending curvature. In other words, it made the actuators less agile. Therefore, these hydrophilic domains helped overcome the limitation of the low water permeability of stiff polymer materials and increased the water-induced bending rate. A 500 μm thick $PIN^{(1/2)}$ actuators is used as a typical example to shown its bending rate (2.5 cm^{-1} within 13 s, Fig. 4C, Movie S1). Moreover, the bent $PIN^{(1/2)}$ actuator gradually reverted to its original shape owing to the reformation of the interlocking cation-π blocks once the moisture had been removed (Fig. 4D). This reversible process was repeated 50 times and recorded maximum curvature of each cycle in various RH. The $PIN^{(1/2)}$ actuators could be bent repeatedly without any apparent fatigue (Fig. S10A and S11) and the stress-strain behavior of the actuator remained essentially the same as that of the original sample (Fig. S10B). To further characterize the stability of the microstructure, phase separation of $PIN^{(1/2)}$ actuator after 50 curling cycles also be studies using

TEM, and the result showed the size of circular ionic domains still maintain approximate 30–50 nm uniformly distributing within the PIN$^{(1/2)}$ (Fig. S12). Thus, the water gradient within the PIN$^{(1/2)}$ actuator and the rapid removal of this water from the actuator surface allowed the actuator to exhibit reversible swelling, which, in turn, caused the actuators to bend and straighten on a moist nonwoven paper substrate (Fig. S13, I to V, Movie S2).

The contractile force and bending stress generated by the PIN$^{(1/2)}$ actuator were measured using a mechanical analyzer. A 500-μm-thick PIN$^{(1/2)}$ actuators was covered with a moist paper and clamped to a universal testing machine (Fig. 5A). A preloading force of 0.05 N was applied to keep the actuator flat and straight. When the moist paper was removed from the PIN$^{(1/2)}$ actuator (Fig. 5B), a contractile force as high as 89 N was recorded. This force can be ascribed to the shrinking and stiffening of the actuators during the water desorption process (Fig. 5C). The corresponding maximum stress was 35.6 MPa, which is approximately 102 times than that of mammalian skeletal muscles (~0.35 MPa). After the PIN$^{(1/2)}$ actuator had been covered again with a moist paper (Fig. 3A), the contractile force reduced to zero as a result of the water-induced swelling and softening of the polymer. A single expansion/contraction cycle took ~8 min. Contractile force of different thick PIN$^{(1/2)}$ actuator (100–600 μm) is a range of 18–102 N and obviously related stress keep ~ 36 MPa (Fig. 5D). Next, to quantify the mechanical force generated by the bending of the polymer actuator, a flat 2 cm long PIN$^{(1/2)}$ actuator (500 μm thick) was placed 2 mm above an electronic balance (Fig. 5E). The top surface of the PIN$^{(1/2)}$ actuator was made moist using steam. This resulted in the actuator bending downward and applying a force on the balance (Fig. 5F). By cutting off the steam flow, the actuator was restored to its original state (Fig. 5E). This was accompanied by a decrease in the force applied on the balance. The force value was read directly from the balance in terms of the weight, which increased and decreased rapidly

within ~4 s (the duration of a single bending/unbending cycle) (Fig. 5G). The maximum weight measured (43 g, which corresponds to a force of 0.43 N) was 107 times higher than the weight of the actuators (400 mg), thus confirming that the stiff PIN$^{(1/2)}$ actuators exhibited excellent mechanical properties in response to the humidity stimuli, which's greatly higher bending force generated and comparable humidity responsive rate than that of the actuators compose of flexible polymer [50-53]. The sturdy, fast-swelling hard actuators could highlight their potential applicability in sensors, switches, and delivery devices that must exhibit high forces. Under the condition that the PIN$^{(1/2)}$ films with different thickness (100–600 μm) has the same curvature in the same atmosphere, bending force of PIN$^{(1/2)}$ actuator is range of 1.2–75 g (Table S2, Fig. 5H), which is 75-128.5 times higher than the weight of the actuators.

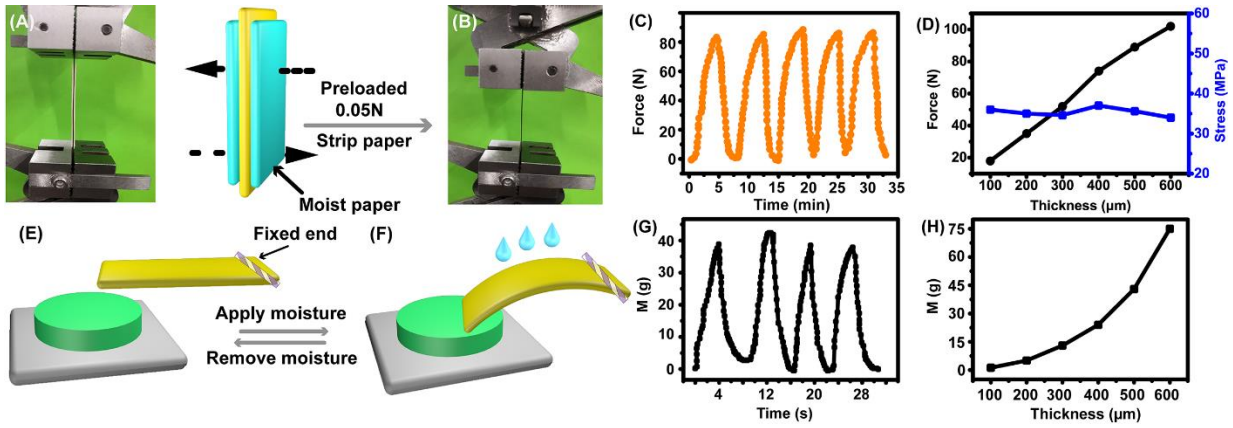

Fig. 5. (A) 500-μm-thick PIN$^{(1/2)}$ actuator was covered by moist paper and clamped to universal testing machine. Preloaded force of 0.05 N was applied to keep sample flat and straight; (B) moist paper was removed and value of contractile force generated was monitored; (C) contractile force generated during humidity sorption and desorption by actuator; (D) contractile force and related stress generated of different thick actuator (100–600 μm); (E) diagrammatic sketch of setup used for measuring force generated in PIN$^{(1/2)}$ actuator, which was fixed at its far end; free end was located above cylinder (green) on electronic balance; (F) force generated by water sorption at actuators surface and after desorption; (G) bending of actuator owing to sorption of water on top surface. Magnitude of force generated was determined in terms of weight reading of balance; (H) bending force of different thick actuator (100–600 μm) with the same degree of bending (2 cm^{-1}) in the method of Fig. 5 EF.

2.5 Transport of cargo system

In addition to exhibiting actuation, actuators often exhibit delicate 3D shapes, which determine their functionality [45,46]. Based on the reversible bending characteristics of the

synthesized epoxy polymer, a PIN$^{(1/2)}$ strip consisting of two actuators attached end to end (weight of each strip: 100 mg) was evaluated for use as a robotic arm for the transport of cargo in factories (Movie S3). For this, we performed the following experiment: first, the PIN$^{(1/2)}$ strip was bent and made to pull an empty toy dump truck (weight of truck: 11 g) to the target loading point by applying water on the top of the surface of film-1 (Fig. 6A, I and II). Next, a weight of 10 g was placed in the truck, and the water on the surface of film-1 was evaporated using flowing air (Fig. 6A, III). Finally, the loaded truck was made to return to the initial point by applying water on the surface of film-2 (Fig. 6A, IV). This process could be repeated several times with ease. The cargo delivery system was found to be efficient, reliable, and reusable using a simple water treatment. Further, the plasticity of the PIN$^{(1/2)}$ actuators used to move the truck is attributable to the phenomenon of a thermoreversible bond exchange (i.e., the aggregation of S-S bonds) [33-36]. This reversible S-S bond exchange within the PIN$^{(1/2)}$ actuator can be spatioselectively programmed to allow for reversible shape changes. For instance, a 2D PIN$^{(1/2)}$ (weight of 100 mg) was shaped into a claw at 120 °C , which is the temperature at which the S-S bond exchange occurs, and an equilibrium conformation is established (Fig. 6B). When the temperature of the PIN$^{(1/2)}$ actuator was reduced to room temperature, the actuator became rigid in the form of a claw (Fig. 6B) and could lift a weight of 10 g successfully when water was applied on its upper surface (Fig. 6C, Movie S4). Thus, the fabricated stiff PIN$^{(1/2)}$ actuator could move a weight of 21 g (210 times greater than the weight of the actuator used) and lift a weight of 10 g (100 times greater than the weight of the actuator used). These values are orders of magnitude higher than those reported previously for similar soft actuator [44-49]. It should be noted that the PIN$^{(1/2)}$ hard actuator exhibited a high thermal decomposition temperature (Fig. S14A, T_d of 330 °C) as well as a high glass transition

temperature (Fig. S14B, T_g of 120 °C). Thus, these PIN$^{(1/2)}$ hard actuators will be highly suitable for use in high-performance hard actuator that must meet stringent performance requirements.

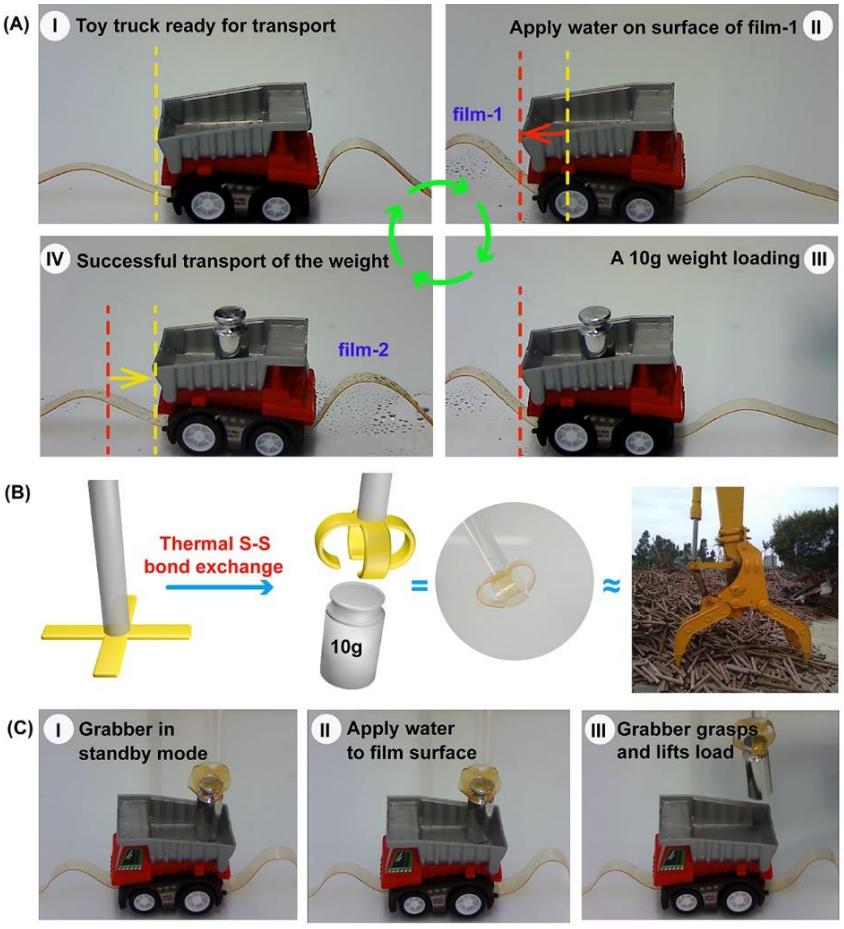

Fig. 6 (A) Robotic arm for delivery of cargo; arm exhibits actuation in response to water; (B) PIN$^{(1/2)}$ actuator shaped into water-responsive claw that can be used for picking/dropping goods; (C) images showing grabbing of weight of 10 g by water-responsive claw.

3. Conclusion

In this study, we combined supramolecular interlocking cation-π blocks, which are dynamic and spatially reconfigurable, with the covalent bonds of a cross-linked epoxy network to synthesize actuators with a stiff polymer network. The synthesized actuators are orders of magnitude stronger that the soft actuator used currently for actuation in soft actuators and exhibit comparable water responsiveness. On the other hand, the stiff epoxy network improves the mechanical properties of the actuator. The use of the synthesized hard actuators in water-driven hard actuators was

demonstrated, thus highlighting their potential applicability in sensors, switches, and delivery devices that must exhibit high forces.

4. Material and methods

4.1 Materials

The monomer tryptophan (98%, cas: 153-94-6), tryptamine (98%, cas: 61-54-1), cystamine dihydrochloride (>97.0% cas: 56-17-7), 2,2-Bis(4-glycidyloxyphenyl) propane (DGEBA) (≥85.0%(GC) on the label, 99.189% in actual), cas: 1675-54-3) were all purchased from J&K chemical and aladdin. All of materials were used without further purification.

4.2 Preparation of cystamine (CTM)

Stir 1 mmol cystamine dihydrochloride and 2.1 mmol sodium hydroxide in water for 10 minutes until hydrochloric acid is completely removed and extracted with dichloromethane (DCM). The combined organic layer was washed with water, dried with anhyd Na_2SO_4, and concentrated under vacuum (Scheme S1).

4.3 Preparation of free-standing epoxy polymer film, PIN(x)

Polymer networks were synthesized by mixing the monomers per the compositions in Table S1. A typical synthetic procedure for $PIN^{(1/2)}$ film with mole ratio 1.00 : 2.00 : 5.00 of Trp-Na^+, CTM and DGEBA is illustrated as an example (Fig. 1A). Before the reaction of Trp-Na^+ with the copolymer, Trp-Na^+ was neutralized with equimolar NaOH in N,N-Dimethylformamide (DMF) to avoid carboxylic acid reacting with epoxy (Scheme S2). The monomer Trp-Na^+, CTM and DGEBA of 1.00 : 2.00 : 5.00 (one film quality 0.5 g) was dissolved in 1.5 ml DMF and stirred to make it mixed evenly. Add small amount of DMF solvent into the mixed solution to make volume about 2 ml. Then the solution was filtered and cast on a clean glass sheet (75mm*25mm), and dried in a convection oven at 80 °C for 6 h and continually in a vacuum at 80 °C, and -0.08 MPa

for 6 h in order to remove a small amount of solvent left. After cooled to room temperature slowly, the samples were cut into the desired dimensions for various testing.

4.4 Curvature calculation

The curling curvature (k) of all actuator strips was monitored and calculated based on the snapshots from movies recorded during humidity-driven curling motions. The radius (r) was measured by software ImageJ. The curvature was calculated as the equation of k = 1 / r.

4.5 Response to Humidity

PIN actuators (25 mm × 5 mm × 0.5 mm) on a moist substrate (moist nonwoven paper containing ~ 30% water by weight) at ambient environment (room temperature 24 °C, relative humidity 50%, no detectable air flow) was recorded by a video camera. With the increase of adsorption time, the curvature of the actuator becomes larger. Record the time when the curvature no longer increases. For a gradient swelling actuator, the relationship between curvature a and thickness n is as follows. This method also be used to screen the length of different thickness actuator in order to ensure the same degree of bending in the same atmosphere compared with 500-μm-thick PIN$^{(1/2)}$ actuators. The detail was shown in Supporting Information:

$$k = \frac{d}{n} \tag{1}$$

4.6 Humidity sorption and desorption

A mini-humidifier was used to provide humid environment. A dry PIN actuator being recorded as m_0 was placed in the humid environment (RH: 99%). Its weight increased by sorption of humidity and was recorded as m at regular intervals. After the actuator was saturated with humidity sorption, it was transferred to a low-humidity environment (RH: 50%). The actuator released water molecules and decreased in its weight. The weight was recorded at regular intervals with the water release. After the actuator returned to the original weight, it was moved to the high-

humid environment again. This operation was repeated three times. The humidity sorption and desorption were analyzed by calculating the variation of the water-sorption ratio with time according to the equation of $(mm_0) / m_0$ mm × 100%. These kinematic processes were analyzed by measuring coiling angles and curling curvatures.

4.7 Locomotion analysis

Locomotion of PIN actuators (15 mm × 15 mm × 0.5 mm) on a moist substrate (moist nonwoven paper containing ~ 30% water by weight) at ambient environment (room temperature 24 °C, relative humidity 50%, no detectable air flow) was recorded by a video camera. The friction between the actuator and substrate affected the locomotion. Hydrophilic substrates with a relatively coarse surface such as paper, cotton clothes and human skin, were good for the actuator's flipping motion. Water evaporation rate dictated the water gradient above the substrate and directly affected actuation of the PIN actuator. At a constant environmental temperature and humidity, and with negligible air-flow, the water evaporation rate was determined by the surface morphology and temperature of the substrate. At low temperatures, the locomotion of a PIN actuator on a moist nonwoven paper was mainly curling and crawling (movie S1).

4.8 Residual elastic potential energy calculation

To characterize the amount of elastic potential energy generated during swelling, the relationship of thickness n and R_E is following:

$$R_E = \frac{E \times w \times d^2 \times n}{2l} \quad (2)$$

where, E, l, w and n refers to the elastic modulus, length, width and depth of PIN. The details was shown in Supporting Information.

4.9 Molecular dynamics (MD) simulation

MD simulation was performed using the amorphous cell module of Materials Studio (Accelrys Software Inc.) with a dreiding force field whose intermolecular parameters were optimized using quantum mechanics. A parent $PIN^{(1/2)}$ chain (as described in Fig. 1B in the main text) with 20 repeating units was built, with 10% repeating units including tryptophan salt (Trp-Na^+) group. Although size of the parent $PIN^{(1/2)}$ chain is not sufficiently long to represent conformations of a real polymer chain, a previous study has reported a good agreement between experiments and simulations when simulated polycarbonate chains are short (merely 10-15 repeat units on average). [54] Moreover, a periodic boundary condition were imposed and an initial density of 0.9 g/cm^3 was used to simulate the polymer conformation in bulk under an equilibrium state. The initial structure was optimized by a molecular mechanics technique using the conjugate gradient method. Because this optimized structure might, however, still be in a local energy minimum state, the polymer in simulation box was relaxed through NVT for 1 ns at 800 K with time steps of 0.2 fs. The simulation of high-temperature relaxation was closely followed a protocol suggested previously. [55] After 1 ns of simulated relaxation at 800 K, the system temperature is decreased to 273 K. In order to obtain a suitable structure for further analysis, ten different initial structures for each system were built and relaxed according to the procedure mentioned previously. The one with the lowest system energy was selected as the MD result for further analysis. MD simulation results in detail was shown in Supporting Information.

4.10 Density functional theory (DFT) calculation

All conformations of both hydrated and nonhydrated indole-complexes have been optimized at the B3LYP/6-31G(d,p) level, and the nature of the resultant stationary points has been ascertained with frequency calculations. Single-point energy calculations have then been performed at the B3LYP/6-311++G(d,p) levels of theory. The simulation procedure was closely

followed a previously suggested one. [40,56] DFT simulation results in detail was shown in Supporting Information.

5. Acknowledgement

Financial support for this work was provided by the National Natural Science Foundation of China (21973076, 11447215, 21202134 and 21504073), the Scientific Research Fund of Science and Technology on Plasma Physics Laboratory (6142A04180411), the Scientific Research Fund of Sichuan Provincial Education Department (18ZA0495 and 16ZA0136), the Sichuan Talent Fund for Distinguished Young Scholars (2021JDJQ0033), the Innovation and Development Fund of China Academy of Engineering Physics (CX20210039), the postgraduate Innovation Fund Project by Southwest University of Science and Technology (20ycx0020), the Student's Platform for Innovation and Entrepreneurship Training Program (S202010619044). Guanjun Chang and Li Yang are grateful for financial support from the China Scholarship Council. We thank the Southwest Computing Center of the China Academy of Physics Engineering for their support of computer simulation. The authors declare no competing financial interests.

6. Conflict of interest

The authors declare no competing financial interest.

7. References

1 J. R. Capadona, K. Shanmuganathan, D. J. Tyler, S. J. Rowan, C. Weder, Stimuli-responsive polymer nanocomposites inspired by the sea cucumber dermis, Science 319 (2013) 1370-1374. https://doi.org/10.1126/science.1153307.

2 J. Song, Y. Zhang, From two-dimensional to three-dimensional structures: A superior thermal-driven actuator with switchable deformation behavior, Chem. Eng. J. 360 (2019) 680-685. https://doi.org/10.1016/j.cej.2018.12.026.

3 L. Ionov, Biomimetic Hydrogel-Based Actuating Systems, Adv. Funct. Mater. 23 (2013) 4555−4570. https://doi.org/10.1002/adfm.201203692.

4 Z. S. Liu, P. Calvert, Multilayer Hydrogels as Muscle-Like Actuator membranes, Adv. Mater. 12 (2010) 288−291. https://doi.org/10.1002/(SICI)1521-4095(200002)12:4<288::AID-ADMA288>3.0. CO; 2-1.

5 H. Yuk, S. T. Lin, C. Ma, M. Takaffoli, N. X. Fang, X. H. Zhao, Hydraulic Hydrogel Actuator membranes and Robots Optically and Sonically Camouflaged in Water, *Nat. Commun.* 8 (2017) 14230. https://doi.org/10.1038/ncomms14230.

6 Z. Zhao, R. Fang, Q. Rong, M. Liu, Bioinspired Nanocomposite Hydrogels with Highly Ordered Structures, Adv. Mater. 29, (2017) 1703045.

7 P. Calvert, Hydrogels for Soft Machines, Adv. Mater. 21 (2009) 743−756. https://doi.org/10.1002/adma.201703045.

8 J. H. Huang, J. X. Liao, T. Wang, W. X. Sun, Z. Tong, Super Strong Dopamine Hydrogels with Shape Memory and Bioinspired Actuating Behaviours Modulated by Solvent Exchange, Soft Matter 14 (2018) 2500−2507. https://doi.org/10.1039/C8SM00297E.

9 D. J. Beebe, J. S. Moore, J. M. Bauer, Q. Yu, R. H. Liu, C. Devadoss, B. H. Jo, Functional Hydrogel Structures for Autonomous Flow Control Inside Microfluidic Channels, Nature 404 (2000) 588−590. https://doi.org/10.1038/35007047.

10 D. T. Eddington, D. J. Beebe, Flow Control with Hydrogels, Adv. Drug Delivery Rev. 56, (2004)199−210. https://doi.org/10.1016/j.addr.2003.08.013.

11 Y. S. Kim, M. J. Liu, Y. Ishida, Y. Ebina, M. Osada, T. Sasaki, T. Hikima, M. Takata, T. Aida, Thermoresponsive Actuation Enabled by Permittivity Switching in an Electrostatically Anisotropic Hydrogel, Nat. Mater. 14 (2015) 1002−1007. https://doi.org/10.1038/nmat4363.

12 Z. F. Sun, Y. Yamauchi, F. Araoka, Y. S. Kim, J. Bergueiro, Y. Ishida, Y. Ebina, T. Sasaki, T. Hikima, T. Aida, An Anisotropic Hydrogel Actuator Enabling Earthworm-Like Directed

Peristaltic Crawling, Angew. Chem., Int. Ed. 57 (2018) 15772−15776. https://doi.org/10.1002/ange.201810052.

13 Y. S. Zhang, A. Khademhosseini, Advances in Engineering Hydrogels, Science 356, (2017) eaaf3627. https://doi.org/10.1126/science.aaf3627.

14 M. Ma, L. Guo, D. G. Anderson, R. Langer, Bio-Inspired Polymer Composite Actuator and Generator Driven by Water Gradients, Science 339 (2013) 186-189. https://doi.org/10.1126/science.1230262.

15 P. Fratzl, F. G. Barth, Biomaterial systems for mechanosensing and actuation, Nature 462 (2009) 442-448. https://doi.org/10.1038/nature08603.

16 X. Qiu, S. Liang, X. Huang, L. Zhang, Pre-patterning and post-oxidation-crosslinking of Fe(0) particles for a humidity-sensing actuator, Chem. Comm. 55 (2019) 15049-15052. https://doi.org/10.1038/nature08603.

17 Y. Li, Y. Sun, Y. Xiao, G. Gao, S. Liu, J. Zhang, F. Jun, Electric Field Actuation of Tough Electroactive Hydrogels CrossLinked by Functional Triblock Copolymer Micelles. ACS Appl. Mater. Interfaces 8 (2016) 26326-26331. https:/doi.org/10.1021/acsami.6b08841.

18 Q. Liu, B. Xu, Solution Evaporation-Driven Crumpling and Assembling of Large Accessible-Space, High-Mechanical-Strength Graphene/Carbon Nanotube. Composite Nanoparticles 12 (2020) 43058-43064. https://doi.org/10.1021/acsami.6b08841.

19 H. Jiang, J. Tang, Zirconium Hydroxide Cross-linked Nanocomposite Hydrogel with High Mechanical Strength and Fast Electro-Response. ACS Appl. Polym. Mater 2 (2020) 3821-3827. https://doi.org/10.1021/acsami.6b08841.

20 J. W. Jung, J. W. Jo, C.-C. Chueh, F. Liu, W. H. Jo, T. P. Russell, A. K.-Y. Jen, Fluoro-Substituted n-Type Conjugated Polymers for Additive-Free All-Polymer Bulk Heterojunction Solar Cells with High Power Conversion Efficiency of 6.71%, Adv. Mater. 27 (2015) 3310-3317. https://doi.org/10.1002/adma.201501214.

21 Y. Sun, L. Qiu, L. Tang, H. Geng, H. Wang, F. Zhang, D. Huang, W. Xu, P. Yue, Y.-S. Guan, F. Jiao, Y. Sun, D. Tang, C.-an Di, Y. Yi, D. Zhu, Flexible n-Type High-Performance Thermoelectric Thin Films of Poly(nickel-ethylenetetrathiolate) Prepared by an

Electrochemical Method, Adv. Mater. 28 (2016) 3351-3358. https://doi.org/10.1002/adma.201505922.

22 N. An, X. Wang, Y. Li, L. Zhang, Z. Lu, J. Sun, Healable and Mechanically Super-Strong Polymeric Composites Derived from Hydrogen-Bonded Polymeric Complexes, Adv. Mater. 31 (2019) 1904882. https://doi.org/10.1002/adma.201904882.

23 E. Filippidi, T. R. Cristiani, C. D. Eisenbach, J. H. Waite, J. N. Israelachvili, B. K. Ahn, M. T. Valentine, Toughening elastomers using musselinspired iron-catechol complexes, Science 358 (2017) 502-505. https://doi.org/10.1126/science.aao0350.

24 A. Dolgopolov, K. N. Grafskaia, D. V. Anokhin, D. E. Demco, X. Zhu, D. A. Ivanov, M. Möllera, Humidity-induced formation of water channels in supramolecular assemblies of wedge-shaped amphiphiles: the effect of the molecular architecture on the channel topology, Phys. Chem. Chem. Phys. 19 (2017) 7714-7720. https://doi.org/10.1039/C6CP08087A.

25 Y. Zhao, J. Yin, Synthesis and evaluation of all-block-sulfonated copolymers as proton exchange membranes for fuel cell application, J. Membrane Sci. 351 (2010) 28-35. https://doi.org/10.1016/j.memsci.2010.01.024.

26 J. Xu, Z. Wang, H. Ni, H. Zhang, A facile functionalized routine for the synthesis of side-chain sulfonated poly(arylene ether ketone sulfone) as proton exchange membranes, Int. J. Hydrogen. Energ. 42 (2017) 5295-5305. https://doi.org/10.1016/j.ijhydene.2016.11.071.

27 K. A. Mauritz, R.B. Moore, State of understanding of Nafion, Chem. Rev. 104 (2004) 4535-4586. https://doi.org/10.1021/cr0207123.

28 J. Li, J. K. Park, R.B. Moore, L.A. Madsen, Linear coupling of alignment with transport in a polymer electrolyte membrane, Nat. Mater. 10 (2011) 507-511. https://doi.org/10.1038/nmat3048.

29 M. Du, L. Yang, X. Luo, K. Wang, G. Chang, Novel phosphoric acid (PA)-poly(ether ketone sulfone) with flexible benzotriazole side chains for high-temperature proton. Polym. J. 51 (2019) 69-75. https://doi.org/10.1038/s41428-018-0118-7.

30 Q. Lu, D. X. Oh, Y. Lee, Y. Jho, D. S. Hwang, H. Zeng, Nanomechanics of Cation-π Interactions in Aqueous Solution, Angew. Chem. Int. Ed. 52 (2013) 4036-4040. https://doi.org/10.1002/anie.201210365

31 A. S. Reddy, H. Zipse, G. N. Sastry, Cation-π Interactions of Bare and Coordinatively Saturated Metal Ions: Contrasting Structural and Energetic Characteristics, J. Phys. Chem. B 111 (2007) 11546-11553. https://doi.org/10.1021/jp075768l.

32 P. Sun, F. Zheng, M. Zhu. Z. Song, K. Wang, M. Zhong, D. Wu, R. B. Little, Z. Xu, H. Zhu, Selective Trans-Membrane Transport of Alkali and Alkaline Earth Cations through Graphene Oxide Membranes Based on Cation−π Interactions, ACS Nano 8 (2018) 850-859. https://doi.org/10.1021/nn4055682.

33 R. Martin, A. Rekondo, A. R. de Luzuriaga, G. Cabãnero, H. J. Grande, I. Odriozola, The processability of a poly(urea-urethane) elastomer reversibly crosslinked with aromatic disulfide bridges, J. Mater. Chem. A 2 (2014) 5710-5715. https://doi.org/10.1039/C3TA14927G.

34 L. Zhang, T. Qiu, Z. Zhu, L. Guo, X. Li, Self-Healing Polycaprolactone Networks through Thermo-Induced Reversible Disulfide Bond Formation, Macromol. Rapid Commun. 39 (2018) 1800121. https://doi.org/10.1002/marc.201800121.

35 T. Li, Z. Xie, J. Xu, Y. Weng, B.-H. Guo, Design of a self-healing cross-linked polyurea with dynamic cross-links based on disulfide bonds and hydrogen bonding, Eur. Polym. J. 107 (2018) 249-257. https://doi.org/10.1016/j.eurpolymj.2018.08.005.

36 X. Wu, J. Li, G. Li, L. Ling, G. Zhang, R. Sun, C.-P. Wong, Heat-triggered poly(siloxane-urethane)s based on disulfide bonds for self-healing application, J. Appl. Polym. Sci. 15 (2018) 46532. https://doi.org/10.1002/app.46532.

37 G. Chang, L. Yang, J. Yang, M. P. Stoykovich, X. Deng, J. Cui, D. Wang, High-Performance pH-Switchable Supramolecular Thermosets via Cation-π Interactions, Adv. Mater. 30 (2018) 1704234. https://doi.org/10.1002/adma.201704234.

38 M. L. Larsen, R. A. Shaw, A. B. Kostinski, S. Glienke, Fine-scale droplet clustering in atmospheric clouds: 3D radial distribution function from airborne digital holography, Phys. Rev. Lett. 121 (2018) 204501. https://doi.org/10.1103/PhysRevLett.121.204501.

39 J. Wilhelm, E. Frey, Radial Distribution Function of Semiflexible Polymers, Phys. Rev. Lett. 77 (1996) 2581. https://doi.org/10.1103/PhysRevLett.77.2581.

40 A. S. Mahadevi, G. N. Sastry, Cation-π Interaction: Its Role and Relevance in Chemistry, Biology, and Material Science, Chem. Rev. 113 (2013) 2100-2138. https://doi.org/10.1021/cr300222d.

41 X. Guan, Y. Ma, L. Yang, Y. Xu, Y. Lan, Y. Huang, T. P. Diangha, G. Chang, Unprecedented toughening high-performance polyhexahydrotriazines constructed by incorporating point-face cation-π interactions in covalently crosslinked networks and the visual detection of tensile strength, Chem. Commun. 56 (2020) 1054-1057. https://doi.org/10.1039/C9CC08603J.

42 H. Yorita, K. Otomo, H. Hiramatsu, A. Toyama, T. Miura, H. Takeuchi, Evidence for the Cation-π Interaction between Cu^{2+} and Tryptophan, J. Am. Chem. Soc. 130 (2008) 15266-15267. https://doi.org/10.1021/ja807010f.

43 J. L. D. Salvo, G. D. Luca, A. Cipollina, G. Micale, Effect of ion exchange capacity and water uptake on hydroxide transport in PSU-TMA membranes: A DFT and molecular dynamics study, J. Membrane Sci. 599 (2020) 117837. https://doi.org/10.1016/j.memsci.2020.117837.

44 S. Liang, X. Qiu, J. Yuan, W. Huang, X. Du, L. Zhang, Multiresponsive kinematics and robotics of surface-patterned polymer film, ACS Appl. Mater. Interfaces 10 (2018) 19123-19132. https://doi.org/10.1021/acsami.8b04829.

45 J. Mu, C. Hou, H. Wang, Y. Li, Q. Zhang, M. Zhu, Origami-inspired active graphene-based paper for programmable instant self-folding walking devices, Sci. Adv. 1 (2015) e1500533. https://doi.org/10.1126/sciadv.1500533.

46 J. Troyano, A. Carné-Sánchez, D. Maspoch, Programmable Self-Assembling 3D Architectures Generated by Patterning of Swellable MOF-Based Composite Films, Adv. Mater. 31 (2019) 1808235. https://doi.org/10.1002/adma.201808235.

47 L. T. De Haan, J. M. N. Verjans, D. J. Broer, C. W. M. Bastiaansen, A. P. H. J. Schenning, Humidity-responsive liquid crystalline polymer actuator membranes with an asymmetry in the molecular trigger that bend, fold, and curl, J. Am. Chem. Soc. 136 (2014) 10585-10588. https://doi.org/10.1021/ja505475x.

48 Y. Dong, J. Wang, X. Guo, S. Yang, M. O. Ozen, P. Chen, X. Liu, W. Du, F. Xiao, Demirci, U.; Liu, B.-F. Multi-stimuli-responsive programmable biomimetic actuator, Nat. Comm. 10 (2019) 1-10. https://doi.org/10.1038/s41467-019-12044-5.

49 L. Zhang, H. Liang, J. Jacob, P. Naumov, Photogated humidity-driven motility. Nat. Comm. 6 (2015) 7429. https://doi.org/10.1038/ncomms8429.

50 Y. Zhang, H. Jiang, F. Li, Y. Xia, Y. Lei, X. Jin, G. Zhang, H. Li, Graphene oxide based moisture-responsive biomimetic film actuators with nacre-like layered structures, J. Mater. Chem. A, 5 (2017) 14604-14610. https://doi.org/10.1039/C7TA04208F.

51 H. Chen, Y. Ge, S. Ye, Z. Zhu, Y. Tu, D. Ge, Z. Xu, W. Chen, X. Yang, Water transport facilitated by carbon nanotubes enables a hygroresponsive actuator with negative hydrotaxis, Nanoscale 12 (2020) 6104-6110. https://doi.org/10.1039/D0NR00932F.

52 G. Xu, M. Zhang, Q. Zhou, H. Chen, T. Gao, C. Lia, G. Shi, A small graphene oxide sheet/polyvinylidene fluoride bilayer actuator with large and rapid responses to multiple stimuli, Nanoscale 9 (2017) 17465-17470. https://doi.org/10.1039/C7NR07116G.

53 Q. He, Z. Wang, Y. Wang, Z. Song, S. Cai, Recyclable and Self-Repairable Fluid-Driven Liquid Crystal Elastomer Actuator, ACS Appl. Mater. Interfaces 31 (2020) 35464–35474. https://doi.org/10.1021/acsami.0c10021.

54 C. F. Fan, T. Cagin, Z. M. Chen, K. A. Smith, Molecular Modeling of Polycarbonate. 1. Force Field, Static Structure, and Mechanical Properties. Macromolecules 27 (1994) 2383-2391. https://doi.org/10.1038/10.1021/ma00087a004.

55 K. J. Lee, W. L. Mattice, R. G. Snyder, Molecular dynamics of paraffins in the n-alkane/urea clathrate. J. Chem. Phys. 96 (1992) 9138-9143. https://doi.org/10.1063/1.462223.

56 A. S. Reddy, H. Zipse, G. N. Sastry, Cation-π interactions of bare and coordinatively saturated metal ions: contrasting structural and energetic characteristics. J. Phys. Chem. B 11 (2007) 11546-11553. https://doi.org/10.1021/jp075768l.